Eur. Phys. J. B **50**, 639–652 (2006)
DOI: 10.1140/epjb/e2006-00171-4

THE EUROPEAN PHYSICAL JOURNAL B

Magnetic field generation by convective flows in a plane layer

O.M. Podvigina[a]

International Institute of Earthquake Prediction Theory and Mathematical Geophysics, 79 bldg. 2, Warshavskoe ave., 117556 Moscow, Russian Federation
and
Laboratory of General Aerodynamics, Institute of Mechanics, Lomonosov Moscow State University, 1, Michurinsky ave., 119899 Moscow, Russian Federation
and
Observatoire de la Côte d'Azur, BP 4229, 06304 Nice Cedex 4, France

Received 10 July 2005 / Received in final form 17 October 2005
Published online 17 May 2006 –

Abstract. Hydrodynamic and magnetohydrodynamic convective attractors in a plane horizontal layer $0 \leq z \leq 1$ are investigated numerically. We consider Rayleigh-Bénard convection in Boussinesq approximation assuming stress-free boundary conditions on horizontal boundaries and periodicity with the same period L in the x and y directions. Computations have been performed for the Prandtl number $P = 1$ for $L = 2\sqrt{2}$ and Rayleigh numbers $0 < R \leq 4000$, and for $L = 4$, $0 < R \leq 2000$. Fifteen different types of hydrodynamic attractors are found, including two types of steady states distinct from rolls, travelling waves, periodic and quasiperiodic flows, and chaotic attractors of heteroclinic nature. Kinematic dynamo problem has been solved for the computed convective attractors. Out of the 15 types of the observed attractors only 6 can act as kinematic dynamos. Nonlinear magnetohydrodynamic regimes have been explored assuming as initial conditions convective attractors capable of magnetic field generation, and a small seed magnetic field. After initial exponential growth, in the saturated regime magnetic energy remains much smaller than the flow kinetic energy. The final magnetohydrodynamic attractors are either quasiperiodic or chaotic.

PACS. 47.20.Ky Nonlinearity, bifurcation, and symmetry breaking – 47.20.Bp Buoyancy-driven instabilities (e.g., Rayleigh-Benard) – 91.25.Cw Origins and models of the magnetic field; dynamo theories

1 Introduction

Thermal convection is a popular area of research. One reason for this is richness and complexity of the system, where different phenomena can be modelled in simulations or investigated employing a variety of mathematical analytical methods (asymptotic, multiscale, equivariant bifurcation theory, etc.). Experiments can be used to verify numerical and theoretical findings. Another reason is physical importance of the problem: convection occurs in nature in many forms and over a wide range of scales. It is believed that magnetic fields of planets and other astrophysical objects are sustained by convective flows of conducting fluid in their interior. For the Earth the hypothesis is supported by computations [1].

Different regimes of thermal convection in a layer in the absence of magnetic field were studied by many authors. For small Rayleigh numbers R (i.e., for small differences in temperature on the horizontal boundaries) the fluid is at rest and heat is transferred by thermal diffusion only. When R exceeds the critical value ($R = 657$ for the boundary conditions under consideration), fluid motion sets in [2]. Without rotation it takes the form of steady rolls [3]. In rotating layer standing or travelling waves also emerge for Taylor and Prandtl (P) numbers in certain ranges [4]. In the non-rotating system stability and bifurcations of convective rolls were studied in the $R - P - q$ space (where q is the wavenumber of the rolls) for rigid [5,6] and stress-free boundaries [7,8]. Stability of some secondary attractors was considered e.g. by Bolton et al. [9], Clever and Busse [10] and Demircan and Seehafer [11]. It was found both experimentally and theoretically that convection in the form of squares or hexagons can coexist with rolls in a parameter range, where only rolls were previously known to be stable [12–14].

Though thermal convection in a layer was extensively explored during the last several decades, detailed results are only available in the vicinity of points of bifurcations, or for the simplest attractors, e.g., convective rolls. To the best of our knowledge, no systematic examination of all time-dependent hydrodynamic attractors of convective motions in a layer was undertaken so far in any parameter region. Imposition of periodic boundary conditions with an apriori fixed period for Rayleigh numbers significantly

[a] e-mail: olgap@mitp.ru

over the critical value is rather restrictive. But it allows one to investigate attractors appearing 'out of blue', e.g. those created in saddle-node bifurcations, or invariant sets (fixed points, orbits or more complex ones) becoming stable as the control parameter is increased, which can not be found otherwise by commonly used local methods.

Magnetic field generation by convective motions in a layer was studied much less. For the trivial steady state (the fluid at rest) generation of magnetic field is, of course, impossible. Without rotation convective rolls cannot generate magnetic field (by virtue of the Zeldovich [15] antidynamo theorem for planar flows), but they can in rotating systems both in kinematic and non-linear regimes [16]. Dynamo was also found if shear was added to the system [17]. Demircan and Seehafer [18] observed magnetic field generation by convective flows of two other types both in the presence or absence of rotation, but in the non-linear regime without rotation the dynamo failed (the hydrodynamic system possesses multiple attractors, and the final state is an attractor incapable of kinematic magnetic field generation). However, in the majority of studies of convection-driven dynamos either extreme parameter values were employed, for which simplified equations could be obtained by asymptotic expansions (for instance, Jones and Roberts [19] and Rotvig and Jones [20] considered the large P limit), or turbulent convection was studied (see Meneguzzi and Pouquet [21] and Cattaneo et al. [22]).

In this paper generation of magnetic field by convective flows is investigated in the simplest setup: We consider fluid heated from below in a plane horizontal layer (it is often regarded as representing a segment of a spherical shell in the interior of a planet). The Boussinesq approximation is assumed, where variation of density is neglected in the mass conservation equation so that the flow is regarded as incompressible. The layer is not rotating. We assume stress-free perfectly conducting horizontal boundaries. Such boundary conditions are commonly used in numerical studies because this seriously simplifies computations and allows one to explore a large range of parameters, apparently not affecting qualitatively results of simulations significantly. (The influence of boundary conditions on convection in the absence of magnetic field and on magnetic field generation by turbulent convection is discussed in [7] and [23], respectively.)

Here, first we study numerically convective attractors. Square space-periodic cells of two sizes L in the horizontal layer $0 \le z \le 1$ are considered. For $L = 2\sqrt{2}$ computations have been performed for Rayleigh numbers $0 < R \le 4000$, and for $L = 4$ – for $0 < R \le 2000$. In both cases Prandtl number is $P = 1$. In the former case rolls are transformed in Hopf bifurcations into a travelling wave and afterwards into modulated travelling waves with several temporal frequencies. In the latter case a more complex sequence of bifurcations takes place, in particular, there exist two types of steady states distinct from rolls, different types of attractors coexist for two windows of R, and chaotic behaviour of heteroclinic nature is observed in another window of R.

Second, we examine magnetic field generation in the linear regime. For $L = 2\sqrt{2}$ magnetic field can be generated by the travelling wave and quasiperiodic flows, the critical magnetic Prandtl number varying from 4.6 to 13. For $L = 4$ out of 14 different types of observed attractors 5 can act as kinematic dynamos.

Third, we investigate non-linear regimes of convection in the presence of magnetic field (with the Lorentz force taken into account). A convective attractor capable of magnetic field generation and a small seed magnetic field are assumed as initial conditions. After initial exponential growth, in the saturated regime magnetic energy remains much smaller on average than the flow kinetic energy. Magnetohydrodynamic (MHD) attractors are either quasiperiodic or chaotic.

2 Statement of the problem

In the absence of magnetic field the system is governed by the Navier-Stokes equation

$$\frac{\partial \mathbf{v}}{\partial t} = \mathbf{v} \times (\nabla \times \mathbf{v}) + P\Delta\mathbf{v} + PR\theta e_z - \nabla p, \qquad (1.a)$$

the incompressibility condition

$$\nabla \cdot \mathbf{v} = 0 \qquad (1.b)$$

and the heat transfer equation

$$\frac{\partial \theta}{\partial t} = -(\mathbf{v} \cdot \nabla)\theta + v_z + \Delta\theta. \qquad (2)$$

Here $\mathbf{v}$ denotes the flow velocity, θ the difference between the flow temperature and the linear temperature profile, and R and P are dimensionless parameters, the Rayleigh number and the Prandtl number, respectively. We assume stress-free boundary conditions for the flow and fixed temperature on horizontal boundaries:

$$\frac{\partial v_x}{\partial z} = \frac{\partial v_y}{\partial z} = v_z = 0, \quad \theta = 0 \quad \text{at } z = 0, 1 \qquad (3)$$

and periodicity in horizontal directions:

$$\mathbf{v}(x, y, z) = \mathbf{v}(x + mL, y + nL, z), \quad \theta(x, y, z) = \theta(x + mL, y + nL, z) \quad (4)$$
$$\forall m, n \in \mathbf{Z}.$$

Magnetic field satisfies the magnetic induction equation

$$\frac{\partial \mathbf{b}}{\partial t} = \nabla \times (\mathbf{v} \times \mathbf{b}) + PP_m^{-1}\Delta\mathbf{b} \qquad (5.a)$$

and the solenoidality condition

$$\nabla \cdot \mathbf{b} = 0. \qquad (5.b)$$

Here P_m is the magnetic Prandtl number. We assume perfectly conducting horizontal boundaries:

$$\frac{\partial b_x}{\partial z} = \frac{\partial b_y}{\partial z} = b_z = 0 \quad \text{at } z = 0, 1 \qquad (6)$$

and periodicity in horizontal directions with the same period as that of the flow:

$$\mathbf{b}(x,y,z) = \mathbf{b}(x+mL, y+nL, z) \quad \forall m,n \in \mathbf{Z}. \qquad (7)$$

When kinematic magnetic field generation is studied, $\mathbf{v}(t)$ is assumed to be a convective attractor. In non-linear regimes magnetic field feedback via the Lorentz force is taken into account, the governing equations being the Navier-Stokes

$$\frac{\partial \mathbf{v}}{\partial t} = \mathbf{v}\times(\nabla\times\mathbf{v}) + P\Delta\mathbf{v} + PR\theta e_z - \nabla p - \mathbf{b}\times(\nabla\times\mathbf{b}), \quad (8)$$

the heat transfer (2) and the magnetic induction (5) equations.

Pseudospectral methods [24] are used to solve the hydrodynamic or MHD systems. A flow $\mathbf{v}$ is represented as a Fourier series:

$$\mathbf{v}^m = \sum_{\mathbf{n}} v_{\mathbf{n}} \mathrm{e}^{\frac{2\pi \mathrm{i}}{L}(n_1 x + n_2 y)} f^m(\pi n_3 z),$$

where $f^m(z) = \cos z$ for $m = 1, 2$ and $f^3(z) = \sin z$. Similar series representations are used for temperature and magnetic field.

Computations have been carried out for $P = 1$. For $L = 2\sqrt{2}$ the Rayleigh number is varied in the range $0 < R \le 4000$ and for $L = 4$, $0 < R \le 2000$. The period $L = 2\sqrt{2}$ corresponds to the horizontal wavenumber $k = \pi/\sqrt{2}$ of the mode which is the first to become unstable for the boundary conditions (3) [2]. For $L = 4$ the most unstable mode is aligned with the diagonal of the periodicity cell. The kinematic dynamo problem (5) has been solved for magnetic Prandtl numbers up to $P_m = 100$. To resolve magnetic field accurately, much higher resolution is necessary than for velocity and temperature fields, since magnetic field has finer structures. Consequently, non-linear regimes of the convective MHD system have been simulated for P_m not exceeding twice the critical value. The resolution of $16\times16\times8$ – $48\times48\times24$ Fourier harmonics is employed for simulation of hydrodynamic convective attractors, and $32\times32\times16$ – $64\times64\times32$ for simulations involving magnetic field either in linear, or non-linear regimes.

3 Symmetries

The symmetry group of the convective system (1), (2) with the boundary conditions (3), (4) is $\mathbf{D}_4 \ltimes \mathbf{T}^2 \times \mathbf{Z}_2$. The 8-element group of symmetries of the square lattice, $\mathbf{D}_4$, is comprised of rotations

$$s_1 : (x,y,z) \mapsto (y,-x,z),$$

$$s_2 : (x,y,z) \mapsto (-x,-y,z),$$

$$s_3 : (x,y,z) \mapsto (-y,x,z),$$

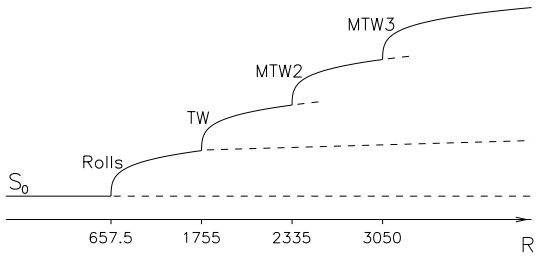

Fig. 1. Bifurcation diagram of the detected attractors of the system (1, 2) for $L = 2\sqrt{2}$ and $0 < R \le 4000$. Labelling of attractors is explained in Section 4.1 (see also Tab. 1). Horizontal axis: Rayleigh number.

reflections

$$s_4 : (x,y,z) \mapsto (x,-y,z),$$

$$s_5 : (x,y,z) \mapsto (-x,y,z),$$

$$s_6 : (x,y,z) \mapsto (y,x,z),$$

$$s_7 : (x,y,z) \mapsto (-y,-x,z)$$

and the identity $s_0 = e$. Elements of the groups $\mathbf{T}_x$ and $\mathbf{T}_y$ of translations in the x and y, respectively, directions are:

$$\gamma_\alpha^x : \ (x,y,z) \mapsto (x+\alpha, y, z)$$

and

$$\gamma_\alpha^y : \ (x,y,z) \mapsto (x, y+\alpha, z)$$

with $0 \le \alpha < L$ ($\gamma_L^x = \gamma_L^y = e$). $\mathbf{T}_{xy}$ denotes the group of translations along the diagonal:

$$\gamma_\alpha^{xy} : \ (x,y,z) \mapsto (x+\alpha, y+\alpha, z).$$

The group $\mathbf{Z}_2$ is generated by reflections about the horizontal midplane:

$$r : \ (x,y,z) \mapsto (x,y,1-z).$$

If magnetic field is present, the group of symmetries of the system also includes the symmetry reversing magnetic field $(\mathbf{v},\mathbf{b}) \to (\mathbf{v},-\mathbf{b})$.

Let $\mathcal{A}$ be an attractor of a dynamical system, invariant under a symmetry g: $g(\mathcal{A}) = \mathcal{A}$. Two cases can be distinguished: either $\mathcal{A}$ is pointwise invariant, i.e. $g(\mathbf{x}) = \mathbf{x}$ for all points $\mathbf{x} \in \mathcal{A}$, or it is invariant only as a set, with $g(\mathbf{x}) \ne \mathbf{x}$ for some $\mathbf{x} \in \mathcal{A}$. In what follows, only symmetries for which an attractor is pointwise invariant are regarded as symmetries of the attractor.

4 Numerical results for L = $2\sqrt{2}$

4.1 Convective attractors

Types of attractors of the system (1)–(4) found in computations are shown on the bifurcation diagram (Fig. 1), for further details see Table 1. Simulations have been carried out for the Rayleigh number incremented step 100 except in the vicinity of bifurcation points, which we identify

Table 1. Attractors, detected in simulations for the hydrodynamic system (1)–(4) for $P = 1$, $L = 2\sqrt{2}$. The fourth column presents the symmetry group for which an attractor is pointwise invariant, the fifth column generators of the group[1]; where a symmetry group is a product of several subgroups, generators of the subgroups are separated by semicolons. The last column presents time-averaged kinetic energy.

Label	Type of the flow	Interval of existence	Group of symmetries	Generators	$\overline{E}_k$
S_0	steady state	$R \leq 657$	$\mathbf{D}_4 \ltimes \mathbf{T}^2 \times \mathbf{Z}_2$	s_1, s_4; γ^x; γ^y; r	0
Rolls	steady state	$658 \leq R \leq 1750$	$\mathbf{D}_2 \ltimes \mathbf{T} \times \mathbf{Z}_2$	s_4, s_5; γ^y; $\gamma^x_{L/2} r$	0–174
TW	periodic, $f_1 = 16.9 \div 17.1$ (travelling wave)	$1760 \leq R \leq 2330$	$\mathbf{D}_2$	$s_5\gamma^y_{L/2}$,$\gamma^x_{L/2} r$	175–209
MTW2	quasiperiodic, $f_1 = 17.0 \div 20.5$, $f_2 = 12.1 \div 14.6$, (modulated travelling wave)	$2340 \leq R \leq 3000$	$\mathbf{Z}_2$	$s_5\gamma^{xy}_{L/2} r$	210–297
MTW3	quasiperiodic, $f_1 = 21.3 \div 25.1$, $f_2 = 14.9 \div 17.9$, $f_3 = 0.8 \div 1.4$ (modulated travelling wave)	$3100 \leq R \leq 4000$	$\mathbf{Z}_2$	$s_5\gamma^{xy}_{L/2} r$	310–446

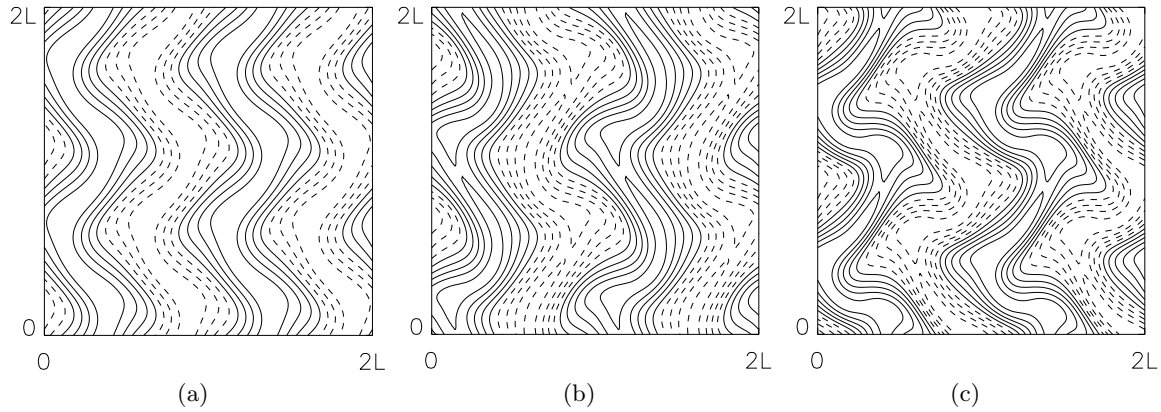

Fig. 2. Isolines (step 5) of v_z on the horizontal midplane $z = \frac{1}{2}$ for $L = 2\sqrt{2}$ and $R = 2300$, TW (a), $R = 2800$, MTW3 (b), $R = 3400$, MTW4 (c). Solid lines indicate positive values, dashed lines – negative values. x – horizontal axis, y – vertical axis.

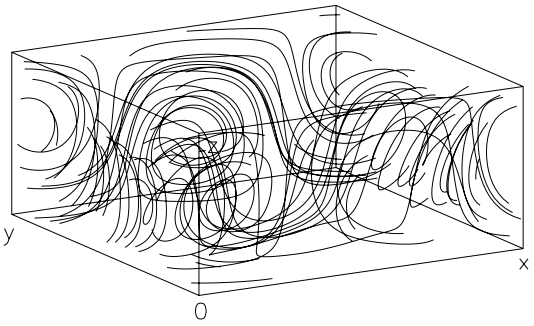

Fig. 3. A sample trajectory in the frame comoving with the TW for $L = 2\sqrt{2}$ and $R = 2300$.

more accurately. Attractors are obtained by continuation in parameter: computations are done with an initial condition, which is a point of the attractor for a smaller R. For each of $R = 2000$, 2400 and 3400 six runs have been performed with random initial perturbations (i.e. perturbations with random Fourier coefficients and an exponentially decaying spectrum) with either small ($\sim 10^{-6}$), or large (~ 100) initial kinetic and thermal energies, but no other attractors have been found.

The trivial steady state (with the fluid at rest) becomes unstable at $R = 657.5$ and fluid motion sets in in the form of steady rolls parallel to x or y coordinate axes, in accordance with [3]. The rolls are stable up to $R = 1750$, afterwards a travelling wave (TW) emerges in a Hopf bifurcation. The instability (called even oscillatory instability in Getling, 1998) results in a sinusoidal bending of the rolls. The pattern travels along the axis of a roll (the y-axis for the flow shown in Fig. 2a). The flow is time-periodic in a coordinate frame at rest and it is

[1] For appropriately chosen location of the origin of the coordinate system. New attractors can be obtained applying symmetries of the system; generators of their symmetry groups should be modified accordingly.

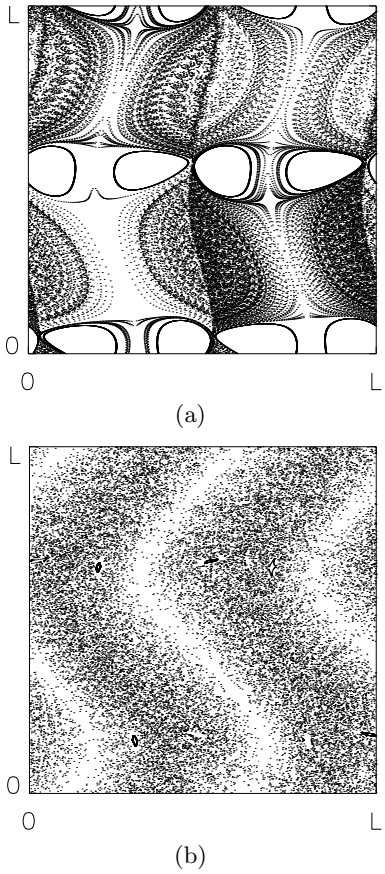

Fig. 4. Poincaré section of the horizontal midplane $z = \frac{1}{2}$ for the flow in the frame comoving with the TW for $L = 2\sqrt{2}$ and $R = 1780$ (a) and $R = 2300$ (b). x–horizontal axis, y–vertical axis.

steady in a frame moving with the speed of the pattern. The flow is chaotic (see Figs. 3 and 4); the area of the plane occupied by chaotic trajectories is large even close to the point of bifurcation from rolls. As R growths, the temporal frequency $f_1(R)$ at first decreases and then increases, attaining the minimum near $R = 2100$. Clever and Busse [10] found similar dependence of the TW frequency on R for convection with rigid horizontal boundaries.

The TW is stable up to $R = 2330$. For $R = 2340$ the attractor is a modulated travelling wave (MTW) which has two basic frequencies (MTW2; see Tab. 1). The next bifurcation at $R = 3050$ is again a Hopf one, in which an MTW with three basic frequencies (MTW3) appears. Spatial structure of MTW2 and MTW3 is more complex than that of TW, but qualitatively the flows are similar (cf. Figs. 2a–c). For modulated travelling waves basic frequencies f_i ($i = 1, 2$ for MTW2 and $i = 1, 2, 3$ for MTW3) increase with R.

4.2 Magnetic field generation

Our computations show that all attractors of the system, except the trivial steady state and unperturbed rolls, can act as dynamos.

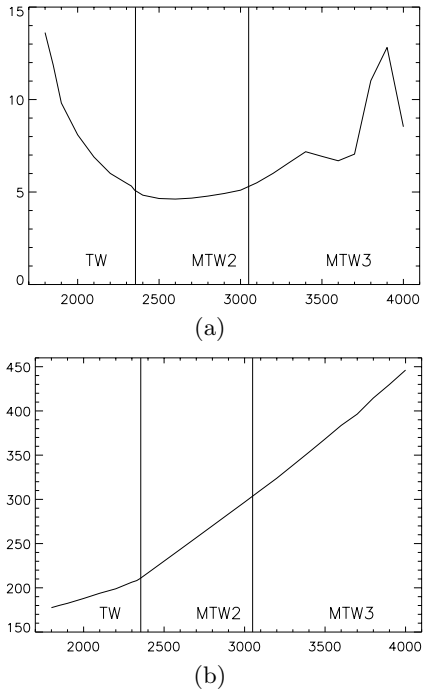

Fig. 5. The critical magnetic Prandtl numbers P_m^c (a) for the magnetic field generation in the linear regime by attractors of the system (1), (2), and time averaged kinetic energy $\overline{E_k}$ (b) of the attractors for $L = 2\sqrt{2}$ and $1800 \le R \le 4000$. Horizontal axis: Rayleigh number.

For MTW2 and MTW3 (5) is solved directly by numerical integration in time (together with (1) and (2) to obtain the convective attractor). If the flow $\mathbf{v}(t)$ in the kinematic dynamo problem is a steady state or a TW, (5) can be reduced to an eigenvalue problem.

Substituting a representation of a TW

$$\mathbf{v}(x, y, z, t) = \mathbf{w}(x + \alpha_x t, y + \alpha_y t, z)$$

moving with the velocity

$$\boldsymbol{\alpha} = (\alpha_x, \alpha_y, 0)$$

into (5) and changing variables

$$(x, y, z) \to (x + \alpha_x t, y + \alpha_y t, z)$$

one finds

$$\frac{\partial \mathbf{b}}{\partial t} = \nabla \times (\mathbf{w} \times \mathbf{b}) - (\boldsymbol{\alpha} \cdot \nabla)\mathbf{b} + PP_m^{-1} \Delta \mathbf{b}.$$

There exist growing magnetic fields, if the eigenvalue problem

$$\lambda \mathbf{b} = \nabla \times (\mathbf{w} \times \mathbf{b}) - (\boldsymbol{\alpha} \cdot \nabla)\mathbf{b} + PP_m^{-1} \Delta \mathbf{b} \qquad (9)$$

has a solution, where the eigenvalue has a pos itive real part. Dominant eigenvalues of (9) are found numerically using the algorithm of Zheligovsky [25].

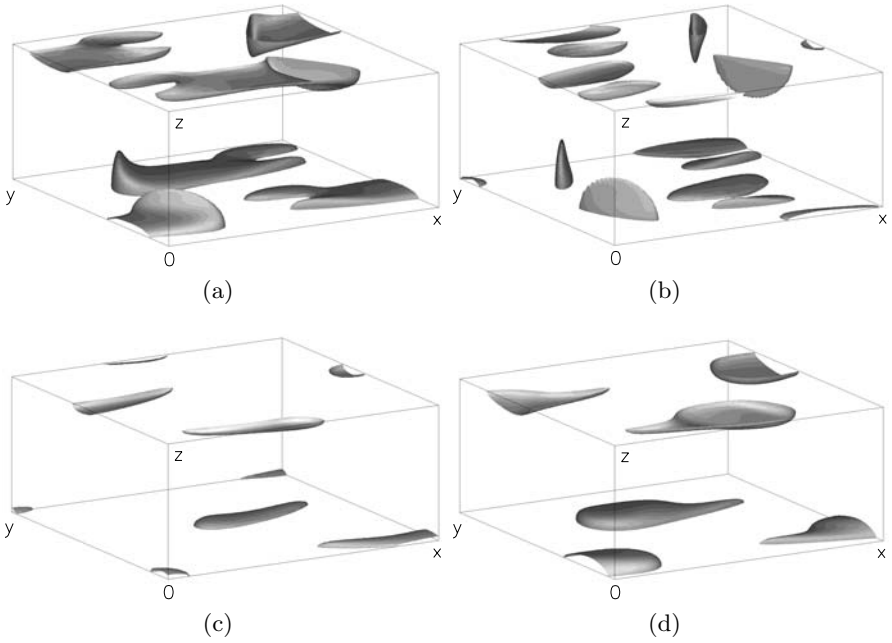

Fig. 6. Isosurfaces at the 50% of the maximal energy density level of the dominant magnetic mode for $L = 2\sqrt{2}$, $R = 2300$ and the critical $P_m^c = 5.33$ (in the frame comoving with the TW). Plots step $\frac{1}{8}$ of the temporal period T of the magnetic mode are shown: $t = 0$ (a), $t = \frac{T}{8}$ (b), $t = \frac{T}{4}$ (c), $t = \frac{3}{8}T$ (d). (The temporal period for the energy is $\frac{T}{2}$).

Critical magnetic Prandtl numbers P_m^c for the onset of magnetic field generation are plotted in Figure 5a. Figure 5b shows time averaged kinetic energy $\overline{E}_k$ for the convective attractors. (The critical magnetic Reynolds numbers can be evaluated as $R_m^c = P_m^c \overline{E}_k^{1/2}$.) Dependence of P_m^c on R is non-monotonous, the minimal $P_m^c = 4.62$ is attained at $R = 2600$ for MTW2. Two local maxima of P_m^c for MTW3 for R close to 3400 and 3900 appear due to exchange of stability between different magnetic modes.

Magnetic field is generated near horizontal boundaries: isosurfaces of magnetic energy density (Fig. 6) are flat half-cigars spread along the boundaries. A similar concentration of magnetic field near horizontal boundaries was observed in convection with rotation by Matthews [16]. Cigar-like magnetic structures are often encountered in dynamo problems for steady flows, which have stagnation points with an one-dimensional unstable manifold; magnetic rope is aligned with the direction of the unstable manifold. Classical numerical examples include magnetic structures generated by ABC flows in the space-periodic geometry [26,27], by Beltrami flows in a sphere [28] and by hexagonal convective cell patterns in a layer [29].

A direct analogy of the structure of magnetic modes satisfying (9) with analytical magnetic rope solutions of Moffatt [30] and Galloway and Zheligovsky [31] could be expected for cigars associated with zeroes of $\mathbf{w} - \boldsymbol{\alpha}$. However, as we have checked, for the attracting TW flows appearing in the present convective system the field $\mathbf{w} - \boldsymbol{\alpha}$ has no stagnation points.

Isosurfaces of small values of the kinetic energy density $|\mathbf{w}|^2$ are plotted in Figure 7a. Cigars in Figure 6 are located near zeroes of $\mathbf{w}$ on the boundaries, no strong magnetic field is generated near zeroes inside the box. The flow velocity on the lower horizontal boundary is plotted in Figure 7b, its structure is inherited from the former rolls: the y-component of the velocity is small, two direct lines of zeroes of rolls modify into S-shaped lines of points where the velocity is small (the vertical component vanishes by virtue of (3)). The cigars and the flow are aligned along the x-axis, magnetic field is maximal in the middle of the cigars halfway between zeroes of the flow.

In the non-linear regime computations have been performed for the following sets of parameters: $R = 2000$, $P_m = 8, 10$; $R = 2300$, $P_m = 8, 10$; $R = 2400$, $P_m = 6, 8, 10$; $R = 3400$, $P_m = 6, 8, 10$; $R = 4000$, $P_m = 8, 10$. Initially magnetic energy grows exponentially, but in the saturated regime it remains smaller than kinetic energy. Attractors are quasi-periodic with several main frequencies, or chaotic (see a typical temporal behaviour of kinetic and magnetic energies in Figs. 8 and 9).

We have not performed computations for higher P_m, because this requires higher resolution. Most computations have been done with $48 \times 48 \times 24$ Fourier harmonics; for this resolution magnetic energy spectrum decreases at least by two orders of magnitude. Some computations have been checked against runs with the resolution $64 \times 64 \times 32$ Fourier harmonics, results remaining unaffected. The flow and temperature energy spectra decrease by about eight orders of magnitude: because of the fine structure of magnetic field more Fourier harmonics are necessary to resolve it adequately.

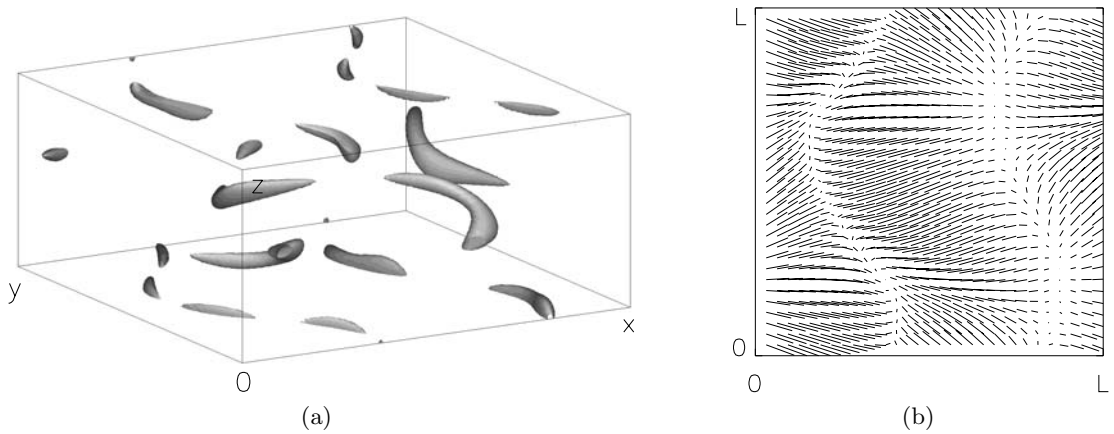

(a) (b)

Fig. 7. Isosurfaces at the 1% of the maximal energy density level of the flow (a) and the flow velocity on the lower boundary $z = 0$ (b, x – horizontal axis, y – vertical axis) (in the frame comoving with the TW) for $L = 2\sqrt{2}$ and $R = 2300$.

Table 2. Attractors, detected in simulations for the hydrodynamic system (1)–(4) for $P = 1$ and $L = 4$. The fourth column presents the symmetry group for which an attractor is pointwise invariant, the fifth column generators of the group; where a symmetry group is a product of several subgroups, generators of the subgroups are separated by semicolons. The last column presents time-averaged kinetic energy.

Label	Type of the flow	Interval of existence	Group of symmetries	Generators	$\overline{E_k}$
S_0	steady state	$R \le 657$	$\mathbf{D}_4 \ltimes \mathbf{T}^2 \times \mathbf{Z}_2$	s_1, s_4; γ^x; γ^y; r	0
SR	steady state	$658 \le R \le 767$	$\mathbf{D}_2 \ltimes \mathbf{T} \times \mathbf{Z}_2$	s_6, s_7; γ^{xy}; $\gamma^x_{L/2} r$	0–14.3
S_1	steady state	$768 \le R \le 783$	$\mathbf{D}_2$	s_6, $s_7 \gamma^{xy}_{L/2} r$	7.8–15.3
P_1	periodic, $f_1^1 = 0.94$	$R = 784$	$\mathbf{Z}_2$	s_6	9.1
Q_1	quasiperiodic, f_1^1, $f_2^1 = 0.12$	$R = 785$	$\mathbf{1}$	e	8.7
C_1	chaotic	$786 \le R \le 812$	$\mathbf{1}$	e	8.1–12.6
P_2	periodic, $f_1^2 = 0.0035 \div 0.01$	$813 \le R \le 815.5$	$\mathbf{1}$	e	9.5–9.8
LR	steady state	$816 \le R \le 897$	$\mathbf{D}_2 \ltimes \mathbf{T} \times \mathbf{Z}_2$	s_4, s_5; γ^y;$\gamma^x_{L/2} r$	9–22
TW	periodic, $f_1^3 = 4.9 \div 5.8$ (travelling wave)	$898 \le R \le 1030$	$\mathbf{D}_2$	$s_5 \gamma^y_{L/2}$, $\gamma^x_{L/2} r$	23–38
MTW2	quasiperiodic, $f_1^3 = 5.8 \div 9.1$, $f_2^3 = 4.7 \div 7.9$, (modulated travelling wave)	$1040 \le R \le 1580$	$\mathbf{Z}_2$	$s_5 \gamma^{xy}_{L/2} r$	39–112
C_2	chaotic	$1590 \le R \le 1670$	$\mathbf{Z}_2$	$s_5 \gamma^{xy}_{L/2} r$	113–123
P_4	periodic, $f_1^4 = 6.9 \div 11.3$	$1200 \le R \le 1930$	$\mathbf{D}_2$	s_2, $s_5 \gamma^{xy}_{L/2} r$	63–167
Q_2	quasiperiodic, $f_1^4 = 11.3 \div 11.6$, $f_2^4 = 4.4 \div 4.6$	$1940 \le R \le 2000$	$\mathbf{D}_2$	s_2, $s_5 \gamma^{xy}_{L/2} r$	168–177
S_2	steady state	$951 \le R \le 1081$	$\mathbf{D}_4$	s_1, s_4	27–45

5 Numerical results for L = 4

5.1 Convective attractors

For $L = 4$ and $0 < R \le 2000$ a more complex sequence of bifurcations has been found in computations than that for $L = 2\sqrt{2}$, discussed in the previous Section (see Fig. 10 and Tab. 2). The Rayleigh number has been increased step 100 except in the vicinity of bifurcation points. Intervals of existence of attractors are determined by continuation in parameter. Six runs with random initial conditions have been performed for each $R = 1000$, 1500 and 2000. Unlike for $L = 2\sqrt{2}$, for $R = 1000$ a new attractor – a steady state S_2 – has been discovered in a run with the new initial conditions.

The trivial steady state becomes unstable at $R = 657.5$ and fluid motion sets in in the form of steady rolls of the spatial period $2\sqrt{2}$, parallel to a diagonal of the periodicity square. These rolls are referred to as "small rolls"

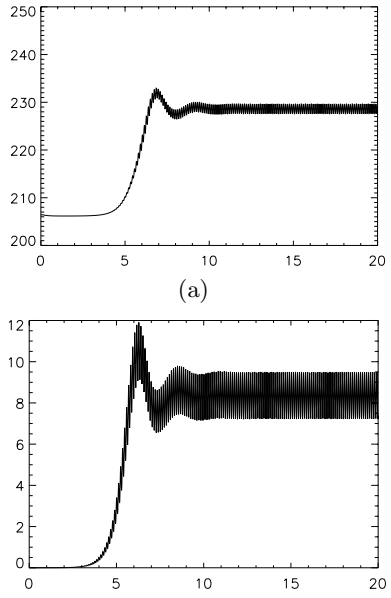

Fig. 8. Kinetic (a) and magnetic (b) energy (vertical axis) as functions of time (horizontal axis) for $L = 2\sqrt{2}$, $R = 2300$ and $P_m = 8$.

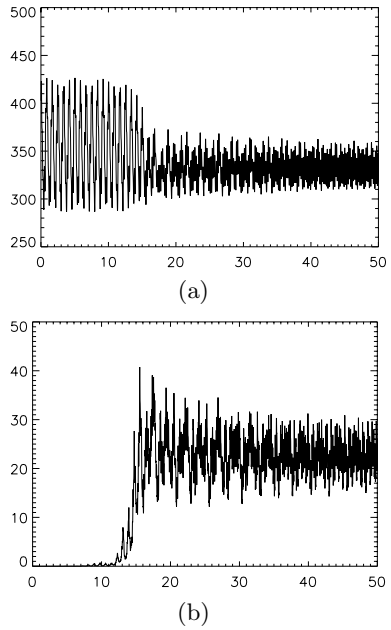

Fig. 9. Kinetic (a) and magnetic (b) energy (vertical axis) as functions of time (horizontal axis) for $L = 2\sqrt{2}$, $R = 3400$ and $P_m = 8$.

(SR) in Tab. 2 in contrast to "large rolls" (LR) of the period $L = 4$ parallel to coordinate axes. Small rolls are stable up to $R = 767$, afterwards a new steady state S_1 emerges in a supercritical bifurcation (see Fig. 11a). The state is called "Asymmetric Squares 2" in the terminology of Proctor and Matthews [32][2]. S_1 becomes unstable in a

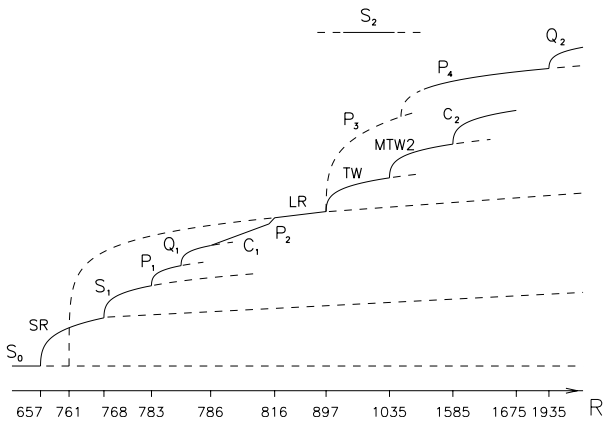

Fig. 10. Bifurcation diagram of the detected attractors of the system (1), (2) for $L = 4$ and $0 < R \leq 2000$. Labelling of attractors is explained in Section 5.1 (see also Tab. 2).

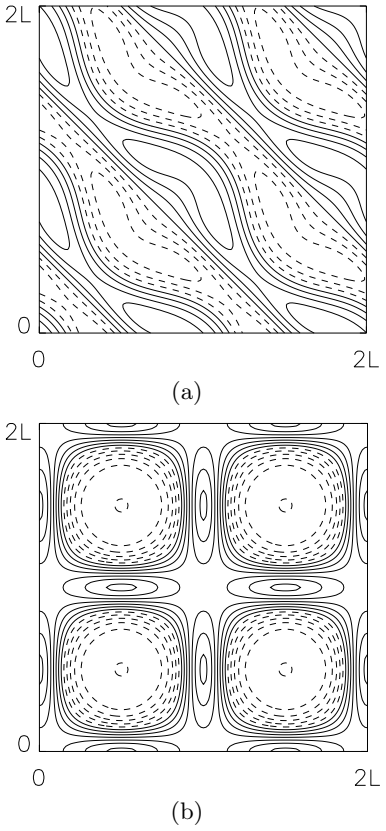

Fig. 11. Isolines (step 1) of v_z on the horizontal midplane $z = \frac{1}{2}$ for $L = 4$: $R = 780$, steady state S_1 (a) and $R = 1000$, steady state S_2 (b). Solid lines indicate positive values, dashed lines – negative values. x–horizontal axis, y–vertical axis.

Hopf bifurcation and a flow with one temporal frequency appears (see Fig. 12a). The next bifurcation is also a Hopf

[2] Proctor and Matthews [32] presented all symmetry types of steady states appearing as a result of the $\sqrt{2}$: 1 steady state mode interaction for non-Boussinesq convection. No similar analysis has been carried out for Boussinesq convection, which has in addition the reflection symmetry and thus admits steady states of other types, e.g. with $A = B$, $C = D = 0$ in the notation *ibid.*

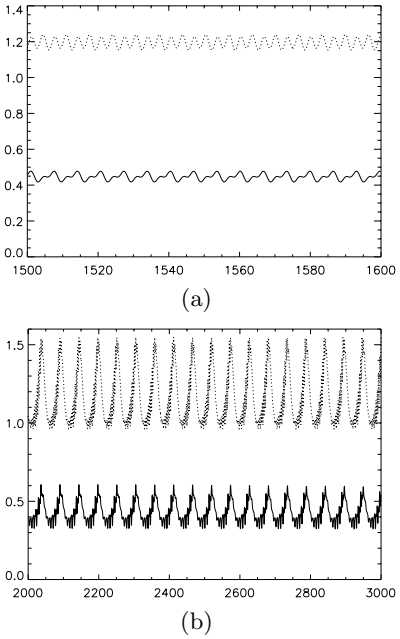

Fig. 12. Fourier coefficient $v^1_{0,1,1}$ (vertical axis) as a function of time (horizontal axis) for $L = 4$: $R = 784$, P_1 (a) and $R = 785$, Q_1 (b). Real part – solid line, imaginary – dotted line.

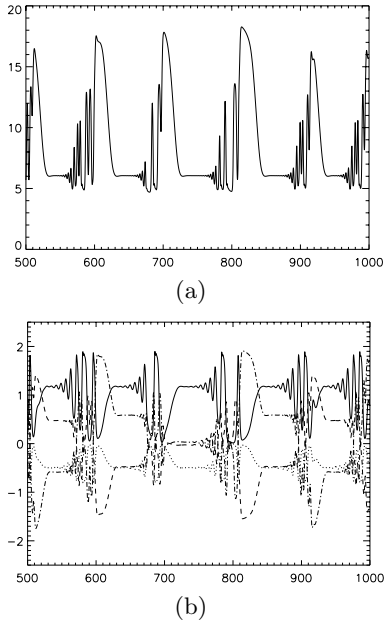

Fig. 13. The energy of the flow (a) and Fourier coefficients (b): $\mathrm{Re}v^2_{0,1,1}$, $\mathrm{Im}v^2_{0,1,1}$, $\mathrm{Re}v^1_{1,1,1}$ and $\mathrm{Im}v^1_{1,1,1}$ (solid, dotted, dashed and dot-dashed lines, respectively) - vertical axis, as functions of time (horizontal axis) for $L = 4$ and $R = 790$.

one, resulting in emergence of the second frequency (see Fig. 12b).

For R in the interval $786 \le R \le 812$, the flow exhibits chaotic behaviour of heteroclinic nature with different types of underlying heteroclinic connections in different subintervals of the interval. Near its lower end a typical temporal behaviour of a trajectory consists of jumps between (unstable) steady states of the type S_1: plateaux of quasiconstant values of the flow energy (Fig. 13a) and the displayed Fourier coefficient (Fig. 13b) correspond to time intervals when the trajectory is close to these steady states. (By steady states of the S_1 (SS, SR, LR) type we call steady states, which can be mapped to S_1 (SS, SR, LR, respectively) by the symmetries of the system). As the Rayleigh number is increased, the time a trajectory spends near S_1 diminishes and the behaviour becomes chaotic and irregular (Fig. 14).

At the upper end of the interval of R, steady states (manifested by plateaux in Fig. 15) distinct from S_1 type ones are visited by a sample trajectory. When $E_k \approx 8$ (e.g. $510 < t < 540$ and $620 < t < 640$), the trajectory is near steady states of the large rolls (LR) type; when $E_k \approx 16$ (e.g. $545 < t < 555$ and $600 < t < 620$), a solution is close to the steady state of the type SS. SS (small squares) can be regarded as a sum of two small rolls of equal amplitude aligned along different diagonals of the periodicity cell. They are discussed in the Appendix. When the flow energy reaches the maxima $E_k \approx 22$ ($t \approx 570$ and $t \approx 770$) the trajectory is close to the SR type flow, and for $t \approx 590$ and $750 < t < 780$, $E_k \approx 19.5$, it visits a steady state of another type S_3, which apparently bifurcates from SR. The time spent near steady states decreases with R decreasing from 812 to 800. However, in

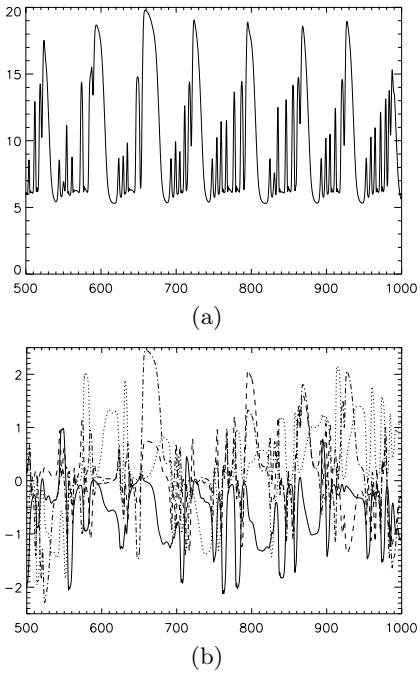

Fig. 14. Same, as in Figure 13, but for $R = 800$.

Figure 14 ($R = 800$) we can still identify time moments when solution is close to LR (e.g. $t \approx 580$) and SS (e.g. $t \approx 585$).

Apparently, for R close to 786, the attractor is located near a heteroclinic cycle connecting the S_1 type flows. The cycle may exist only for an isolated value of R. For R close to 812 the attractor resides near a heteroclinic network

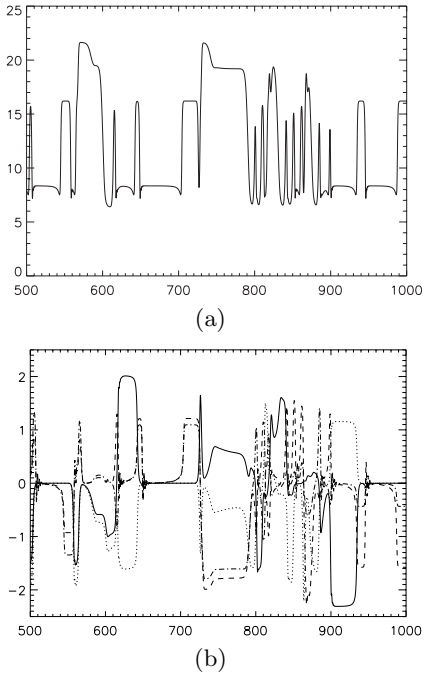

Fig. 15. Same, as in Figure 13, but for $R = 812$.

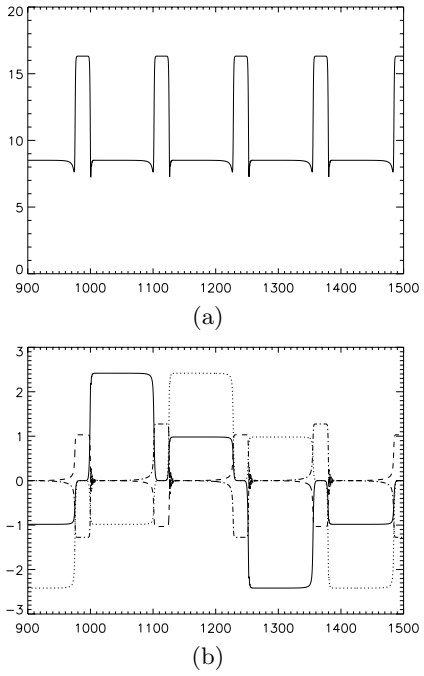

Fig. 16. Same, as in Figure 13, but for $R = 813$.

connecting the LR, SR, SS and S_3 types solutions. (A part of the network connecting LR's and SS's is constructed in the Appendix). In the middle of the interval none of the heteroclinic structures are attracting, a trajectory is close to steady states for short times. It seems impossible to indicate a precise boundary between the three patterns of behaviour on the interval of R under discussion; apparently each pattern continuously evolves into the next one.

For $813 \leq R \leq 815.5$ (see Fig. 16) the behaviour is periodic: a periodic orbit emerges apparently from a heteroclinic cycle, which is a subset of a heteroclinic network connecting steady states of the LR and SS types (see Appendix). Denote by $\mathrm{LR}_\alpha = \gamma_\alpha^x \mathrm{LR}_0$ rolls obtained by the shift by α in the x direction and by $\mathrm{SS}_\alpha = \gamma_\alpha^{xy}\mathrm{SS}_0$ small squares obtained by the shifts by α in x and y directions; note $\mathrm{SS}_{L/2} = \mathrm{SS}_0$. The heteroclinic cycle connects steady states in the following order: $\mathrm{LR}_0 \to \mathrm{SS}_0 \to \mathrm{LR}_{L/4} \to \mathrm{SS}_{L/4} \to \mathrm{LR}_{L/2} \to \mathrm{SS}_0 \to \mathrm{LR}_{3L/4} \to \mathrm{SS}_{L/4} \to \mathrm{LR}_0 \to \ldots$ As always for cycles created from a heteroclinic or homoclinic connection, its temporal period decreases when the distance (in the parameter space) to the point of bifurcation increases.

For $816 \leq R \leq 897$ the attractors are the large rolls (initially unstable when they bifurcate from S_0 at $R = 761$). At $R = 897$ the LR become unstable in a Hopf bifurcation and a TW emerges, similarly to the bifurcation of rolls for $L = 2\sqrt{2}$ when those become unstable (Fig. 17a). The next bifurcation at $R = 1035$ is also similar to the $L = 2\sqrt{2}$ case – it is a Hopf bifurcation resulting in emergence of MTW2. At $R = 1585$ the behaviour becomes chaotic, the attractor C_2 persists up to $R = 1670$. For higher R trajectories are attracted by a time-periodic orbit P_4.

The orbit P_4 has been traced down to $R = 1200$; for smaller R it is unstable and trajectories initially close to P_4 are attracted by MTW2. For $R < 1200$ computations were performed with the s_2 symmetry imposed and with P_4 as initial condition. The computations reveal that P_4 appears at $R = 1050$ in a pitchfork bifurcation from a periodic orbit P_3 (see Fig. 10), which is always unstable. The P_3 symmetry group, $\mathbf{Z}_2^3$, is generated by s_2, $s_5\gamma_{L/2}^y$ and $\gamma_{L/2}^x r$. It bifurcates from LR simultaneously with the TW. At the point of bifurcation the symmetries $s_5\gamma_{L/2}^y$ and $\gamma_{L/2}^x r$ act trivially on the center eigenspace of (1)–(2) linearised in the vicinity of LR (this was checked numerically). Thus, the action of the LR symmetry group on the center eigenspace is isomorphic to $\mathbf{O}(2)$. Golubitsky et al. [34] have studied analytically a Hopf bifurcation with the $\mathbf{O}(2)$ symmetry group. They found that standing and rotating (or, in the present context, travelling) waves bifurcate simultaneously; if both branches are supercritical, one of them is stable. Our numerical results agree with their theory. The difference between the symmetries of TW and P_3 (standing wave) is illustrated by Figure 18. Note, that for TW imaginary part of the coefficient $v^1_{1,1,1}$ is shifted by a quarter of the time period relative real part, since TW possesses the so-called spatio-temporal symmetry $\gamma_\alpha^x \gamma_\phi^t$ with $\phi = -2\pi\alpha/(f_1^3 L)$ (here γ_ϕ^t denotes shift in time by ϕ).

At $R = 1935$ a second frequency appears. The attractor is a torus with two main frequencies.

Runs with random initial conditions have revealed that the system possesses another attractor S_2, unrelated to the sequence of attractors described above. It is a steady

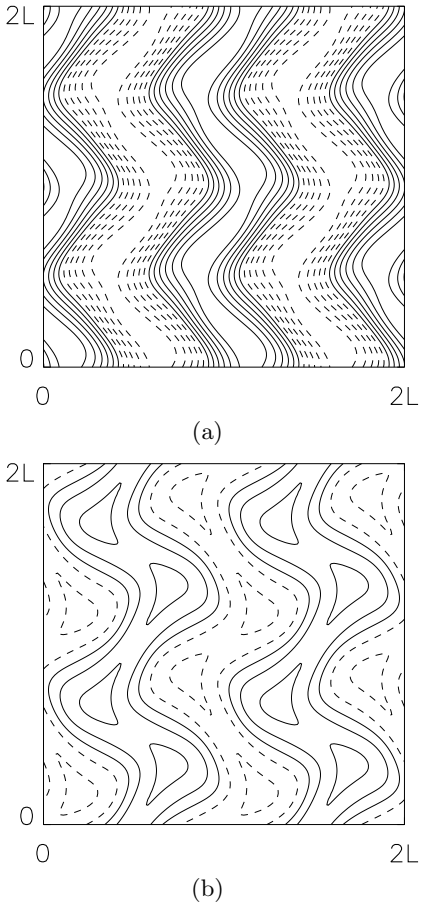

Fig. 17. Isolines of v_z on the horizontal midplane $z = \frac{1}{2}$ for $L = 4$: $R = 1000$ (step 1), TW (a) and $R = 1400$ (step 5), P_4 (b). Solid lines indicate positive values, dashed lines – negative values. x – horizontal axis, y – vertical axis.

state with the symmetry group D_4 of the periodicity square. In the terminology of [32] this steady state is "Large Squares". The flow consists of cells of the period L, where fluid is rising near boundaries and descending at the centre (see Fig. 11b). Application of the symmetry r yields a flow whose direction is reversed. S_2 exists for $951 \le R \le 1081$, no attractors bifurcate from it for smaller or larger R. Demircan and Seehafer (2002) also observed it in computations for $P = 6.8$ and $3.5 \le L \le 5$.

5.2 Magnetic field generation in linear and non-linear regimes

The kinematic dynamo problem (5) has been considered for all attractors, listed in Table 2, except for the trivial steady state and rolls. We find that TW, P_4 and all subsequent attractors can act as kinematic dynamos, and the remaining attractors do not generate magnetic field for $P_m \le 100$.

The obtained critical Prandtl numbers P_m^c are plotted in Figure 19a. The values are larger compared to those for $L = 2\sqrt{2}$ (cf. Figs. 6a and 19a). A possible reason is that

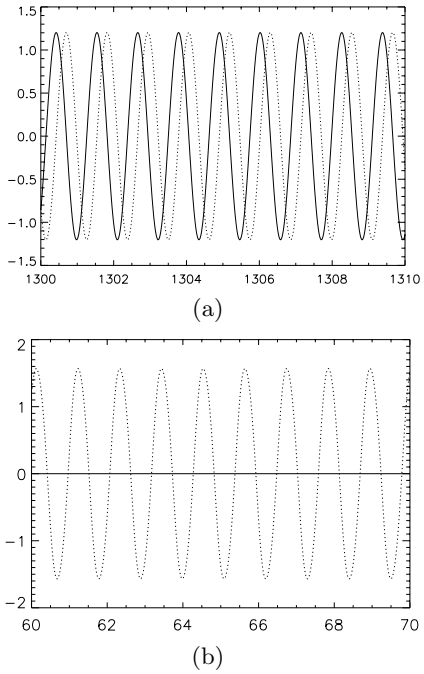

Fig. 18. Fourier coefficient $v^1_{1,1,1}$ (vertical axis) as a function of time (horizontal axis) for $L = 4$ and $R = 1000$: TW (a) and P_3 (b). Real part – solid lines, imaginary – dotted lines. For P_3 real part vanishes due to the imposed symmetry s_2.

the energy of convective attractors is smaller for $L = 4$ (cf. Figs. 6b and 19b); the respective critical magnetic Reynolds numbers $R_m^c = P_m^c \overline{E}_k^{1/2}$ differ less. The local maximum of P_m^c is due to exchange of stability between different magnetic modes.

Non-linear regimes have been investigated for $R = 1000$, $P_m = 16$; $R = 1200$, $P_m = 20$; $R = 1500$, $P_m = 18$; $R = 2000$, $P_m = 18$ (initial conditions in simulations being, respectively, the TW, MTW2, P_4 or Q_2 and a small seed magnetic field). The regimes are similar to those for $L = 2\sqrt{2}$: Initially magnetic energy grows exponentially, but in the saturated regime it remains smaller than kinetic energy. Attractors are quasi-periodic with several main frequencies, or chaotic (a typical temporal behaviour of kinetic and magnetic energies is displayed in Fig. 20).

6 Conclusion

The convective system (without magnetic field) possesses a rich variety of attractors. We have identified fifteen types of convective flows, including steady states, travelling waves, regimes involving several temporal frequencies. The computations were performed for the Prandtl number $P = 1$ (compressed gases used in recent experiments often have $P \approx 1$ [35]). Despite some simplifications of the considered system, i.e. stress-free horizontal boundaries and imposed periodicity in horizontal directions, there are some common features with experimental observations. Travelling waves, present for both considered values of L in computations, was observed by Cakmur

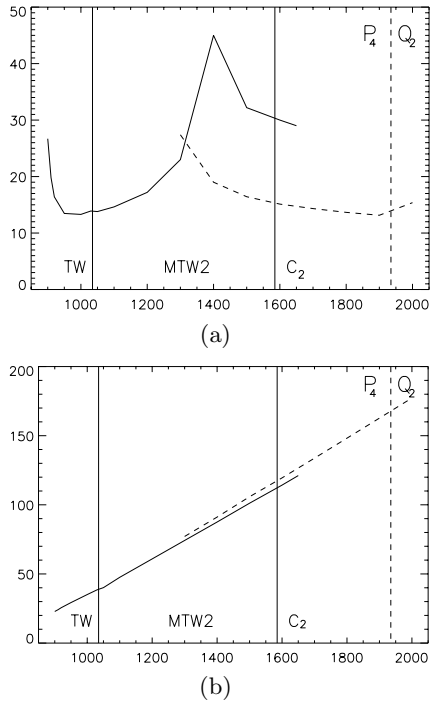

Fig. 19. Critical magnetic Prandtl numbers P_m^c (a) for the onset of magnetic field generation by attractors of the system (1), (2) and time averaged kinetic energy of the attractors $\overline{E}_k$ (b) for $L = 4$ and $900 \leq R \leq 2000$. Horizontal axis: Rayleigh number. Plots for attractors TW, MTW2 and C_2 are shown by solid lines, for P_4 and Q_2 by dashed lines.

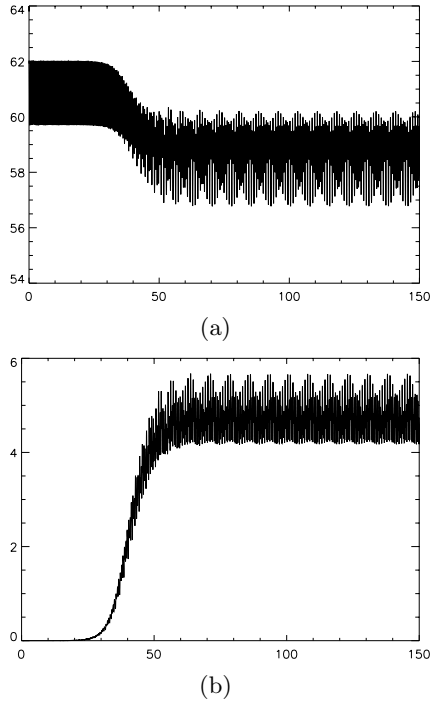

Fig. 20. Kinetic (a) and magnetic (b) energy (vertical axis) as functions of time (horizontal axis) for $L = 4$, $R = 1200$ and $P_m = 20$.

et al. [36]. Coexistence of several types of attractors (as in Fig. 13, bifurcation diagramm for $L = 4$) was also reported in experiments (see references in [35]). Spiral-defect chaos (complex spatio-temporal dynamics involving different kinds of patterns observed for $R > 1.26R_c$) may be related to a heteroclinic connection, similar to the one found for $L = 4$ and $786 \leq R \leq 812$.

Out of fifteen types of convective attractors six can act as kinematic dynamos. Magnetic field, if generated kinematically, persists in non-linear regime.

The study has been performed for two different values of the aspect ratio. For both employed values, if Rayleigh number is large enough, the respective convective attractors can generate magnetic field. The property of a convective attractor to be a kinematic dynamo is inherited by attractors bifurcating from it – e.g. TW is a kinematic dynamo, and so are MTW2 and MTW3. We observe a non-monotonous dependence of the critical P_m on R. The best magnetic field generators (the ones, where generation starts at the smallest P_m) among convective attractors are travelling waves MTW2 for $R = 2600$ (for $L = 2\sqrt{2}$) and TW for $R = 1000$ (for $L = 4$). Magnetic field concentrates near the horizontal boundaries. In all MHD simulations reported here magnetic energy is much smaller than the kinetic one, because computations have been carried out for P_m not far from its critical value.

For both considered values of L, the largest Fourier coefficients are those corresponding to rolls with the periods L and $L/\sqrt{2}$ (the ones aligned with a coordinate axis or along diagonals of periodicity cells), indicating that analytical investigation of the $1{:}\sqrt{2}$ resonance in a system with the $\mathbf{D}_4 \ltimes \mathbf{T}^2 \times \mathbf{Z}_2$ symmetry group is necessary to understand convective bifurcations reported here. This work is in progress. We intend to examine a general system with this symmetry group and the particular system obtained from (1), (2) by the center manifold reduction, similarly to the study of bifurcations in the ABC forced hydrodynamic system [37,38]. This investigation will reveal as well, which bifurcations can occur for other parameter values not considered in this paper. Mode interaction is responsible for the heteroclinic connection observed for $R \sim 815$ (see Appendix). The nature of chaotic behaviour for $786 \leq R \leq 812$ apparently will be also clarified by this investigation.

I am grateful to Profs S.Ya. Gertsenshtein and A. Soward, to Drs A. Gilbert and V. Zheligovsky for discussions, and to an anonymous referee for his stimulating remarks. Codes of Zheligovsky (1993) were used for eigenvalue computations. Part of this research was carried out during my visits to the School of Mathematical Sciences, University of Exeter, UK, in May–July 2002 and in January–April 2004. I am grateful to the Royal Society for their financial support. Some numerical results were obtained using computational facilities provided by the program "Simulations Interactives et Visualisation en Astronomie et Mécanique (SIVAM)" at Observatoire de la Côte d'Azur, France. My research visits to Observatoire de la Côte d'Azur were supported by the French Ministry of Education.

This work has been partly financed by the grant from the Russian Foundation for Basic Research 04-05-64699.

Appendix: Heteroclinic network in a system with the 1:$\sqrt{2}$ mode interaction

In this Appendix we consider the 1:$\sqrt{2}$ mode interaction to show that structurally stable heteroclinic connection between solutions of the SS and LR types is possible. This particular mode interaction is important, because the ratio of periods of the first two modes becoming unstable (rolls along the diagonal and along the edges of the periodicity cell) is 1:$\sqrt{2}$. Such connection can be responsible for the behaviour observed for $L = 4$, $813 \le R \le 815.5$.

The notation of [32] is used. A solution of (1, 2) restricted to the center manifold is represented as

$$h(x,y) = \mathrm{Re}(Ae^{ix} + Be^{iy} + Ce^{i(x+y)} + De^{i(x-y)}).$$

The symmetries of the system (see Sect. 3) transform the complex amplitudes A, B, C and D in the following way:

$$\begin{aligned}
s_1 &: (A,B,C,D) \to (B,\bar{A},\bar{D},C),\\
s_4 &: (A,B,C,D) \to (A,\bar{B},D,C),\\
s_5 &: (A,B,C,D) \to (\bar{A},B,\bar{D},\bar{C}),\\
\gamma^x_\alpha &: (A,B,C,D) \to (e^{i\alpha}A,B,e^{i\alpha}C,e^{i\alpha}D),\\
\gamma^y_\alpha &: (A,B,C,D) \to (A,e^{i\alpha}B,e^{i\alpha}C,e^{-i\alpha}D),\\
r &: (A,B,C,D) \to (-A,-B,-C,-D).
\end{aligned}$$

Amplitude equations, invariant under the action of the symmetry group of the system, truncated at cubic order have the form

$$\begin{aligned}
\dot{A} &= \mu_1 A - A(\lambda_1|A|^2 + \lambda_2|B|^2\\
&\quad + \lambda_3(|C|^2 + |D|^2)) - \nu_1\bar{A}CD,\\
\dot{B} &= \mu_1 B - B(\lambda_1|B|^2 + \lambda_2|A|^2\\
&\quad + \lambda_3(|C|^2 + |D|^2)) - \nu_1\bar{B}C\bar{D},\\
\dot{C} &= \mu_2 C - C(\lambda_4|C|^2 + \lambda_5|D|^2\\
&\quad + \lambda_6(|A|^2 + |B|^2)) - \nu_2(B^2D + A^2\bar{D}),\\
\dot{D} &= \mu_2 D - D(\lambda_4|D|^2 + \lambda_5|C|^2\\
&\quad + \lambda_6(|A|^2 + |B|^2)) - \nu_2(\bar{B}^2C + A^2\bar{C}).
\end{aligned} \tag{10}$$

Unlike in [32], the quadratic terms are absent due to the Boussinesq symmetry r.

The subspace $(x_1, 0, x_2, x_2)$ is a fixed-point subspace for the group generated by s_4, s_5 and $\gamma^x_{L/2}r$. The subspace contains the LR solutions

$$(A,B,C,D) = \pm(\mu_1/\lambda_1)^{1/2}(1,0,0,0)$$

and the SS solutions

$$(A,B,C,D) = \pm(\mu_2/(\lambda_4+\lambda_5))^{1/2}(0,0,1,1)$$

(assuming $\mu_1/\lambda_1 > 0$ and $\mu_2/(\lambda_4+\lambda_5) > 0$). The eigenvalues controlling stability of LR are $-2\mu_1$ and $\mu_2 - (\lambda_6+\nu_2)\mu_1/\lambda_1$ associated with the eigenspaces $(1,0,0,0)$ and $(0,0,1,1)$, respectively, and the eigenvalues controlling stability of SS are $-2\mu_2$, $\mu_1 - (2\lambda_3+\nu_1)\mu_2/(\lambda_4+\lambda_5)$ associated with the eigenspaces $(0,0,1,1)$ and $(1,0,0,0)$. The bifurcations to both large rolls and small squares are supercritical, therefore $\mu_1 > 0$ and $\mu_2 > 0$. If $\mu_2 - (\lambda_6+\nu_2)\mu_1/\lambda_1 < 0$ and $\mu_1 - (2\lambda_3+\nu_1)\mu_2/(\lambda_4+\lambda_5) > 0$, LR is stable in this subspace, SS is unstable, and a connection from SS to LR is possible. Since this is a fixed-point subspace for a subgroup of of $\mathbf{D}_4 \ltimes \mathbf{T}^2 \times \mathbf{Z}_2$, according to Proposition 2.5 in [39] the connection is robust.

Similarly, the subspace $(x_1, 0, ix_2, ix_2)$ is a fixed-point subspace for the group generated by s_4, $\gamma^y_{L/2}s_5$ and $\gamma^x_{L/2}r$. It contains the same LR solutions $\pm(\mu_1/\lambda_1)^{1/2}(1,0,0,0)$ and the SS solutions $\pm i(\mu_2/(\lambda_4+\lambda_5))^{1/2}(0,0,1,1)$. The eigenvalues controlling stability of LR are $-2\mu_1$ and $\mu_2 - (\lambda_6-\nu_2)\mu_1/\lambda_1$, with the associated eigenspaces $(1,0,0,0)$ and $(0,0,i,i)$, respectively, and the eigenvalues controlling stability of SS are $-2\mu_2$, $\mu_1 - (2\lambda_3-\nu_1)\mu_2/(\lambda_4+\lambda_5)$ associated with eigenspaces $(0,0,i,i)$ and $(1,0,0,0)$. If $\mu_2 - (\lambda_6-\nu_2)\mu_1/\lambda_1 > 0$ and $\mu_1 - (2\lambda_3-\nu_1)\mu_2/(\lambda_4+\lambda_5) < 0$, a robust connection from LR to SS is possible.

These connections underline the switching between the SS and LR type flows observed in Figure 16. However, application of the $\mathbf{D}_4 \ltimes \mathbf{T}^2 \times \mathbf{Z}_2$ symmetries reveals that multiple heteroclinic trajectories approach and leave each of the SS and LR types steady states. We do not address here the question why the trajectory chooses the particular path of the network.

Heteroclinic connections in (10), described above, reside in the invariant subspace $(A, 0, C, C)$. Dynamical system (10) restricted on this invariant subspace is identical to the one, for which the $\mathbf{O}(2) \times \mathbf{Z}_2$ mode interaction was investigated in [40,41]. Conditions for existence of structurally stable heteroclinic connections in the restricted system were found in these papers. The cycle (existing for appropriate values of the coefficients) connects steady states of the types $(A,0,0,0)$ and $(0,0,C,C)$, similarly to the ones found above. However, heteroclinic cycles found here and in [40,41] are different. In [40,41] it involves 8 steady states: $(A,0,0,0) \to (0,0,C,C) \to (iA,0,0,0) \to (0,0,iC,iC) \to (-A,0,0,0) \to (0,0,-C,-C) \to (-iA,0,0,0) \to (0,0,-iC,-iC) \to (A,0,0,0)$, while we observe in Figure 16 connection between 6 steady states: $(A,0,0,0) \to (0,0,C,C) \to (iA,0,0,0) \to (0,0,i\bar{C},i\bar{C}) \to (-A,0,0,0) \to (0,0,C,C) \to (-iA,0,0,0) \to (0,0,i\bar{C},i\bar{C}) \to (A,0,0,0)$.

References

1. G.A. Glatzmaier, P.H. Roberts, Nature **377**, 203 (1995)
2. S. Chandrasekhar, *Hydrodynamic and Hydromagnetic Stability* (Dover, 1981)
3. A. Schluter, D. Lortz, F. Busse, J. Fluid Mech. **146**, 115 (1984)
4. E. Knobloch, M. Silber, Geophys. Astrophys. Fluid Dynamics **51**, 195 (1990)
5. F.H. Busse, Rep. Prog. Phys. **41**, 1929 (1978)

6. F.H. Busse, in *Mantle Convection: Plate Tectonics, Global Dynamics*, edited by W.R. Peltier 23 (1989)
7. F.H. Busse, E.W. Bolton, J. Fluid Mech. **146**, 115 (1984)
8. E.W. Bolton, F.H. Busse, J. Fluid Mech. **150**, 487 (1985)
9. E.W. Bolton, F.H. Busse, R.M. Clever, J. Fluid Mech. **164**, 469 (1986)
10. R.M. Clever, F.H. Busse, J. Fluid Mech. **176**, 403 (1987)
11. A. Demircan, N. Seehafer, Europhys. Lett. **53**, 202 (2001)
12. M. Assenheimer, V. Steinberg, Phys. Rev. Lett. **76**, 756 (1996)
13. R.M. Clever, F.H. Busse, Phys. Rev. E **53**, 2037 (1996)
14. F.H. Busse, R.M. Clever, Phys. Lett. **81**, 341 (1998)
15. Ya.B. Zeldovich, Journ. Exper. Theor. Phys. **31**, 154 (1956); Engl. transl.: Sov. Phys. J.E.T.P. **4**, 460 (1957)
16. P.C. Matthews, Proc. R. Soc. **455**, 1829 (1999)
17. F. Busse, J. Fluid Mech. **57**, 529 (1973)
18. A. Demircan, N. Seehafer, Geophys. Astrophys. Fluid Dynamics **96**, 461 (2002)
19. C.A. Jones, P.H. Roberts, J. Fluid Mech. **404**, 311 (2000)
20. J. Rotvig, C.A. Jones, Phys. Rev. E **66**, 056308 (2002)
21. M. Meneguzzi, A. Pouquet, J. Fluid Mech. **205**, 297 (1989)
22. F. Cattaneo, T. Emonet, N. Weiss, Astrophysical Journal **588**, 1183 (2003)
23. J.-C. Thelen, F. Cattaneo, Mon. Not. R. Astron. Soc. **315**, L13 (2000)
24. J.P. Boyd, *Chebyshev and Fourier Spectral Methods* (Springer-Verlag, Berlin 1989)
25. V. Zheligovsky, J. Scientific Comput., **8** (1), 41 (1993)
26. D.J. Galloway, U. Frisch, Geophys. Astrophys. Fluid Dynamics **29**, 13 (1984)
27. D.J. Galloway, U. Frisch, Geophys. Astrophys. Fluid Dynamics **36**, 53 (1986)
28. V.A. Zheligovsky, Geophys. Astrophys. Fluid Dynamics **73**, 217 (1993)
29. V.A. Zheligovsky, D.J. Galloway, Geophys. Astrophys. Fluid Dynamics **88**, 277 (1998)
30. H.K. Moffatt, *Magnetic Field Generation in Electrically Conducting Fluids* (Cambridge University Press, 1978)
31. D.J. Galloway, V.A. Zheligovsky, Geophys. Astrophys. Fluid Dynamics **76**, 253 (1994)
32. M.R.E. Proctor, P.C. Matthews, Physica D **97**, 229 (1996)
33. D. Armbruster, J. Guckenheimer, P. Holmes, Physica D **29**, 257 (1988).
34. M. Golubitsky, I.N. Stewart, D. Schaeffer, *Singularities and Groups in Bifurcation Theory. Volume 2*, Appl. Math. Sci. **69** (Springer-Verlag, New York, 1988)
35. E. Bodenschatz, W. Pesch, G. Ahlers, Annu. Rev. Fluid Mech. **32**, 709 (2000)
36. R.V. Cakmur, D.A. Egolf, B.B. Plapp, E. Bodenschatz, Phys. Rev. Lett. **79**, 1853 (1997)
37. O.M. Podvigina, accepted in Dynamical Systems (2005)
38. O. Podvigina, P. Ashwin, D. Hawker, accepted in Physica D (2005)
39. M. Krupa, I. Melbourne, Ergodic Theory Dyn. Syst. **15**, 121 (1995)
40. P. Hirschberg, E. Knobloch, Chaos **3**, 713 (1993)
41. P. Hirschberg, E. Knobloch, Nonlinearity **11**, 89 (1998)